Eur. Phys. J. A **11**, 161–173 (2001)

THE EUROPEAN PHYSICAL JOURNAL A

Emission of $^{8}Be_{gs}$ in the interaction of ^{12}C with nuclei at incident energies up to 33 MeV/amu

E. Gadioli[1,a], G.F. Steyn[2], C. Birattari[1], M. Cavinato[1], S.H. Connell[3], A.A. Cowley[4], E. Fabrici[1], S.V. Förtsch[2], E. Gadioli Erba[1], J.J. Lawrie[2], F.M. Nortier[2], J.P.F. Sellschop[3], and E. Sideras Haddad[3]

[1] University of Milano and INFN, Sezione di Milano, Milano, Italy
[2] National Accelerator Centre, Faure, South Africa
[3] Schonland Research Centre, Witwatersand University, Johannesburg, South Africa
[4] Department of Physics, University of Stellenbosch, Private Bag XI, Matieland 7602, South Africa

Received: 3 May 2001
Communicated by R.A. Ricci

Abstract. The spectra of $^{8}Be_{gs}$ fragments emitted in the interaction of 100, 200, 300 and 400 MeV ^{12}C with ^{59}Co, ^{93}Nb and ^{197}Au have been measured and analysed. Our analysis suggests that, before breaking up, ^{12}C may suffer a considerable energy loss which increases with increasing incident energy. The amount of excitation energy provided to the target nucleus in this process increases with decreasing charge of the target nucleus.

PACS. 25.70.Gh Compound nucleus – 25.70.Mn Projectile and target fragmentation

1 Introduction

Many studies have interpreted the very forward emission of projectile fragments in the interaction of light ions with nuclei as a direct process produced by peripheral interactions. In this *scenario* different mechanisms have been introduced, but a definitive agreement on its interpretation has not yet been reached. These mechanisms include: a) binary projectile fragmentation with both fragments escaping without further interacting with the target nucleus [1–3] (in the present paper, this mechanism will be called elastic break-up); b) transfer of the unobserved fragment to the target (also called break-up fusion) [3–5]; c) processes where the projectile undergoes a dissipative interaction with the target before breaking up [6–8]; d) processes where the fragment undergoes a final-state interaction before emission [9,10]. In particular, McVoy and Nemes [3] showed that a local-momentum plane-wave Born approximation (PWBA) (equivalent to the well-known Serber approximation in light-particle break-up [11,12]) in which the projectile and the observed fragment momenta are locally corrected for the Coulomb repulsion reproduces the spectra of a heavy fragment reasonably well (*e.g.*, ^{12}C produced in the interaction of ^{16}O with ^{208}Pb at incident energies ranging from 140 to 315 MeV [13]). This approach was originally formulated for describing elastic break-up processes. However, in a subsequent paper, Hussein *et al.* [9] suggested that, since any final-state interaction of the unobserved fragment cannot alter the spectrum of the observed fragment, it may be used for describing the inclusive spectra of a fragment, including all the possible final-state interactions of the unobserved fragment. They also reconsidered the data analysed in ref. [3] and showed that at an incident energy of 315 MeV, better agreement is attained if it is assumed that the observed fragment undergoes a final-state interaction. This improvement is most notable in the lower-energy region, where the break-up spectra display longer tails than expected solely on the basis of the PWBA. The energy degraded and broadened spectrum resulting from such an interaction was evaluated by folding the break-up spectrum with the inelastic scattering spectrum of the observed fragment. This yielded a more satisfactory reproduction of the experimental spectra. However, the spectra still show a low-energy component which previous approaches do not reproduce and which Hussein *et al.* [9] assumed to be due to some complex pre-compound processes unrelated to the break-up contribution.

The observation of unstable fragments like ^{8}Be may be useful to clarify this matter since it presents three invaluable advantages in comparison to the observation of stable or long-lived fragments. The first is that, due to the fact that the experimental technique requires the coincident measurement of two correlated α-particles, the resulting ^{8}Be spectra are not contaminated by contributions of other Be isotopes. In contrast, the measurement of

[a] e-mail: gadioli@mi.infn.it

stable fragments, such as, *e.g.*, ^{12}C fragments produced in ^{16}O break-up, will not usually resolve other adjacent C isotopes. The second advantage is that the ^{8}Be ground state can easily be separated from the first and higher-excited states, whereas as will be explained below, in the case of stable or long-lived fragments one cannot normally distinguish contributions of different excited states. Thirdly, since $^{8}Be_{gs}$ is unbound, it is unlikely to survive a final-state interaction. Therefore, it is improbable that a reduction of its emission energy and a broadening of its emission energy distribution is due to such final-state interactions.

Guided by these considerations, in a previous study, we have analysed the spectra of $^{8}Be_{gs}$ fragments produced in the interaction of ^{12}C with ^{59}Co at incident energies of 100 and 400 MeV [14]. We found that, at the most forward angles, the shape of the $^{8}Be_{gs}$ spectra is characteristic of ^{12}C elastic break-up. However, at the highest incident energy, the $^{8}Be_{gs}$ average energy was notably smaller than that corresponding to the beam velocity and the spectrum width, which in an elastic break-up should reflect the momentum distribution of the fragment within the projectile, was distinctly larger than expected. As discussed before, this could be due either to an initial-state interaction of the projectile with the target nucleus, leading to a reduction and a spreading of its energy before break-up, and/or to a reduction of the observed fragment energy in a final-state interaction. However, since $^{8}Be_{gs}$ is unbound and most presumably cannot survive a final-state interaction, we suggested that the reduction of its energy and its broader energy distribution were rather due to an initial-state interaction.

In this paper, we present an extended set of data concerning the production of $^{8}Be_{gs}$ in the interaction of ^{12}C with i) ^{59}Co at incident energies of 200 and 300 MeV (in addition to the data at 100 and 400 MeV already presented [14]) and with ii) ^{93}Nb and ^{197}Au at incident energies of 100, 200, 300 and 400 MeV. Since these two nuclei have mass and charge considerably higher than that of ^{59}Co, these data, together with those previously discussed, allow one to study the dependence of the alleged interaction on the incident energy and the target charge. We will show that the experimental data are quite reasonably reproduced by a modified version of the McVoy-Hussein approach assuming, as already suggested [14], that the observed reduction of the energy of $^{8}Be_{gs}$ fragments and the broadening of its emission spectra are due to an initial-state interaction of the projectile with the target, instead of to a final-state interaction of the emitted fragments.

The experimental procedures are described in sect. 2, the results are presented and discussed in sect. 3, followed by the conclusions, presented in sect. 4.

2 Experimental procedure

The pioneering work performed at the University of Edinburgh in the construction of high-efficiency ^{8}Be detection systems utilizing silicon strip detectors (SSDs) [15–17] proved to be very useful for the present study. Since ^{8}Be is unbound, the identification of these nuclei when formed in their lower-lying states involves the detection of two correlated decay α-particles. In order to measure ^{8}Be nuclei produced in their ground state with kinetic energies up to 400 MeV, we employed SSDs in conjunction with conventional stopping detectors. This allowed for proper identification and energy determination of ^{8}Be reaction products over a wide region of emission energy, from about 40 MeV up to 400 MeV. A detailed account of these detector systems, their performance characteristics and Monte Carlo modelling will be given elsewhere [18], therefore only a brief description is given here.

Beams of ^{12}C ions of 100, 200, 300 and 400 MeV nominal energy and 200 MeV α-particles were supplied by the cyclotron facility of the National Accelerator Centre (NAC), Faure, South Africa. The beams were focused to a spot size on target of about 3 mm in diameter. Beam offsets were determined by comparing the yield from elastic scattering on either side of the beam axis. The beam halo was monitored in the usual way by comparing count rates produced by a target and by an empty target frame at regular intervals. Beam intensities were such that the electronic dead time remained below 1% at all times.

Targets of ^{59}Co, ^{93}Nb and ^{197}Au with thicknesses of respectively 1.00, 1.72 and 0.483 mg/cm^2 were used. These targets were mounted in aluminium frames with 25 mm diameter apertures, which again were mounted on an aluminium target ladder that fits onto a target drive mechanism at the centre of the large NAC scattering chamber.

Two detector telescopes were mounted on rotatable arms on opposite sides of the beam axis, in the same reaction plane. Each telescope consisted of a single double-sided SSD as a ΔE detector, followed by a single NaI stopping E detector. This configuration allowed us to obtain ΔE information for both correlated α-particles constituting ^{8}Be, but not the total energy for each of them individually. The total ^{8}Be energy (*i.e.* the sum energy of the two α-particles) could however be uniquely determined.

The SSDs used in this experiment have 16 vertical anode strips and 16 horizontal cathode strips each, with an active area of 50 mm $\times$ 50 mm. The inter-strip gaps are 100 μm in width. Individual strip readouts were provided for all the vertical strips, while the horizontal strips were bussed together to give only two readouts, one for even-numbered strips and one for odd-numbered strips. This required 18 independent channels of electronic instrumentation per SSD. Several detector thicknesses were utilized, depending on the incident beam energy. For the 400 MeV measurements, 500 μm thick detectors were used while 280 μm thick detectors were used at 200 and 300 MeV. The measurements at 100 MeV required a somewhat different strategy which will be described later. The distance from the centre of the target to the centre of the front face of a SSD was 467 mm, the maximum allowed by the dimensions of the scattering chamber and the detector assemblies.

The stopping detectors used have NaI(Tl) crystals of 3 inch in diameter and 2 inch thickness. These detectors have HAVAR entrance windows of 2.5 inch in diameter and 7 μm thickness. From a perspective looking towards

the target from behind a telescope, silicon strips 1 and 16 are partially obstructed by the front window flange of a NaI detector. Brass collimators with 2.5 inch apertures and 7 mm thickness were therefore placed between the SSDs and the NaI detectors to prevent α-particles from being degraded by the window flanges from entering the NaI crystals.

A two-fold coincidence was normally required in hardware between any of the vertical silicon strips in order to generate event and trigger, but it was also possible to collect data in single mode. Conventional ΔE-E particle identification (PID) spectra were generated for each vertical strip in coincidence with a NaI stopping detector. Since good ^{8}Be events yield ΔE signals of individual α-particles but E signals for the sum of the two correlated α-particles, these α-particles lie on a different kinematic locus than the single α-particles which are observed when collecting data in single mode. Software gates were set around these ^{8}Be loci during the data analysis.

The detector telescopes were calibrated by utilizing the kinematics of elastic scattering of 200 MeV α-particles from deuterated polythene targets. During these runs it was also noted that a small percentage of elastically scattered α-particles gave signals in two adjacent silicon strips. This appears to happen for some single α-particles when a SSD is traversed through an inter-strip gap, and can be attributed to the well-known phenomenon of positive + positive charge sharing [17]. Since these single α-particles can in principle mimic low-energy ^{8}Be events, it was decided to discard coincidence events when adjacent strips "fired". An indication of slit scattering was also observed for silicon strips 1 and 16. Although this did not appear to be serious, we decided to use only strips 2 through 15 in the final data analysis since the resulting detector efficiency was still high enough for our purposes. In principle, it is also possible to recover a large fraction of the true ^{8}Be events where both α-particles traversed the same vertical strip but different horizontal strips, yielding both odd and even signals. The trigger logic should then also include those events in which signals are detected not only in one vertical strip but also in both the odd and even horizontal channels. Although this is what we initially intended to do, we eventually decided to forfeit these events in order to simplify the analysis and to avoid possible contributions from single α-particles giving signals in adjacent horizontal strips, even though this spurious contribution would probably have been rather small.

Standard fast coincidence electronics and an online computer were used to acquire and store the event data stream. The computer dead time was automatically corrected for by means of a *busy* output which was used as a veto signal in the electronic processing. The gains of the NaI detectors were monitored by means of prescaled pulsers triggering light-emitting diodes (LEDs) implanted in the crystals. This enabled corrections to be made for gain drifts in these detectors. Data were acquired at mean scattering angles of 7°, 9°, 12°, 16° and 20°.

The effective solid angles were calculated using the break-up Monte Carlo program UNIMONTE [19] and are shown as a function of ^{8}Be kinetic energy in fig. 1. Since the mean separation angle of the outgoing α-particles increases with increasing separation energy, the detector efficiency is much higher for the 0^{+} ground state (E_{s} = 0.092 MeV) than for the 2^{+} first excited state (E_{s} = 3.13 MeV) [20]. Consequently, the measured ^{8}Be spectra are dominated by the ground state. The mean separation angle also decreases with increasing ^{8}Be emission energy, therefore these detectors are more efficient for higher ^{8}Be energies.

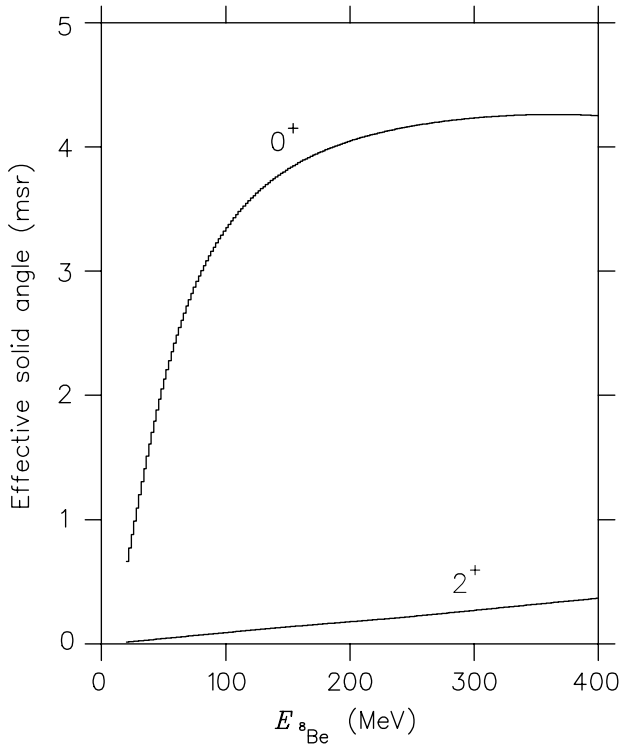

Fig. 1. Effective solid angles for detection of ^{8}Be with the detector system described in the text. Monte Carlo calculations were performed for the 0^{+} ground state and 2^{+} first excited state of ^{8}Be.

In this work, our primary objective was to measure continuum emission spectra for ^{8}Be formed in the ground state. The yields of the first excited state therefore pose as a contaminant for the ground-state spectra. In addition to the favourable magnitude of the detection efficiency for the ground state relative to that for the first excited state, the ΔE information for the individual decay α-particles provides a further means to separate a large fraction of the observed first-excited-state yield from the ground-state yield. We generated two-dimensional histograms of $(\Delta E_1 - \Delta E_2)$ *versus* $(\Delta E_1 + \Delta E_2)$. In these spectra one observes different loci for the ground and first excited states, and by setting a software gate some of the first-excited-state yield can be removed. However, due to partial overlap of these loci a clean separation is not possible. Nevertheless, the remaining contamination is quite small, estimated to be well below 5% in all the data measured. At the lowest incident energy of this study, *i.e.* 100 MeV, the use of the SSDs as ΔE detectors resulted

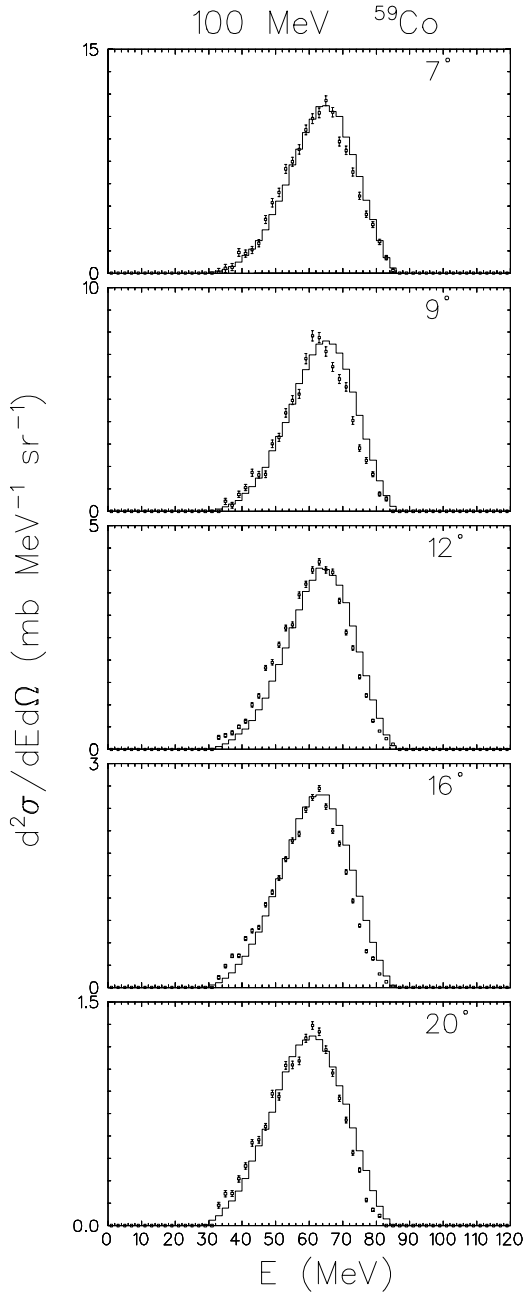

Fig. 2. Spectra of $^{8}Be_{gs}$ emitted between 7° and 20° in the interaction of 100 MeV ^{12}C with ^{59}Co. The experimental data are given by the open squares with error bars. The calculated break-up spectra are given by the continuous line histograms.

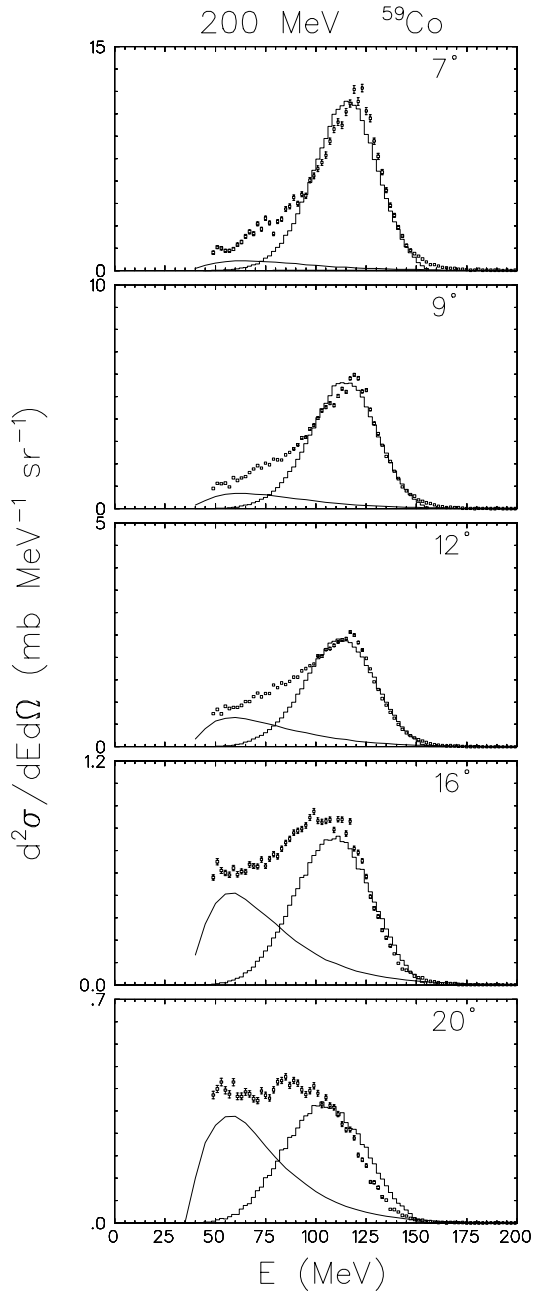

Fig. 3. Spectra of $^{8}Be_{gs}$ emitted between 7° and 20° in the interaction of 200 MeV ^{12}C with ^{59}Co. The experimental data are given by the open squares with error bars. The calculated break-up and coalescence spectra are given by, respectively, the histograms and the continuous lines.

in a too high lower limit of detection to observe the full break-up peak in the measured ^{8}Be emission spectra. In this case we therefore used a 1 mm thick SSD as an E detector and the NaI detector as a veto detector. As before, a two-fold coincidence between any of the vertical strips was required to generate an event trigger. Fortunately, in the $(\Delta E_1 - \Delta E_2)$ *versus* $(\Delta E_1 + \Delta E_2)$ spectra similar characteristic ^{8}Be loci were observed as at the other incident energies and the ^{8}Be events could still be satisfactorily extracted by setting a single software gate.

3 Results and discussion

3.1 Overview of the experimental results

The measured $^{8}Be_{gs}$ spectra, including those already presented in [14], are shown in figs. 2 to 5 for the ^{59}Co target, in figs. 6 to 9 for the ^{93}Nb target and in figs. 10 to 13 for the ^{197}Au target. In this last case the $^{8}Be_{gs}$ spectra were only measured at 12°, 16° and 20° at 100 MeV and at 12° at 200 MeV. The experimental results are given by the open

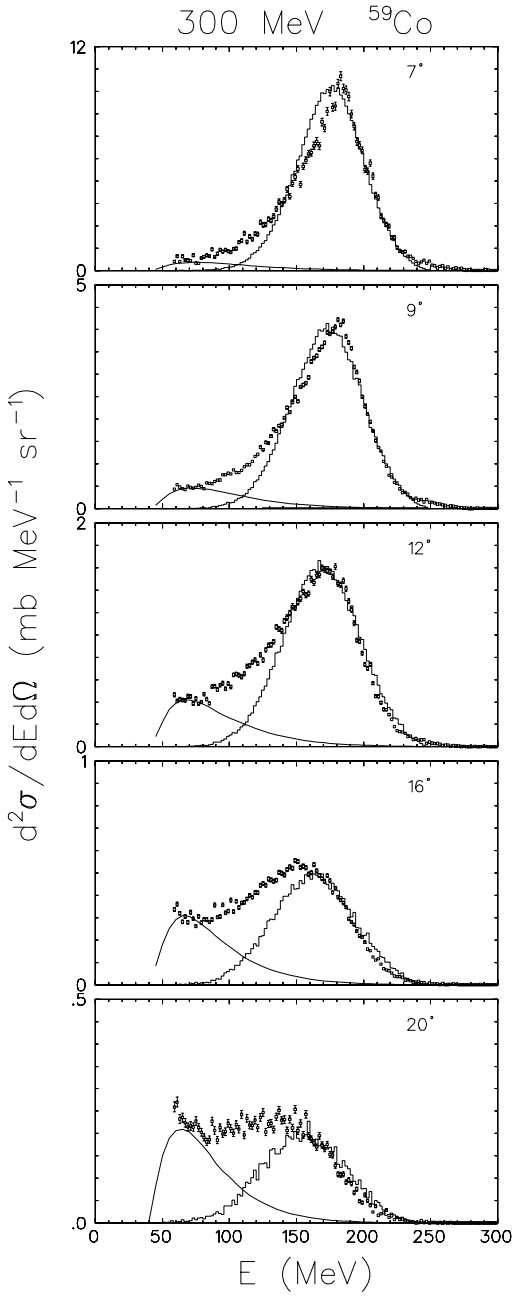

Fig. 4. Spectra of $^{8}Be_{gs}$ emitted between 7° and 20° in the interaction of 300 MeV ^{12}C with ^{59}Co. The experimental data are given by the open squares with error bars. The calculated break-up and coalescence spectra are given by, respectively, the histograms and the continuous lines.

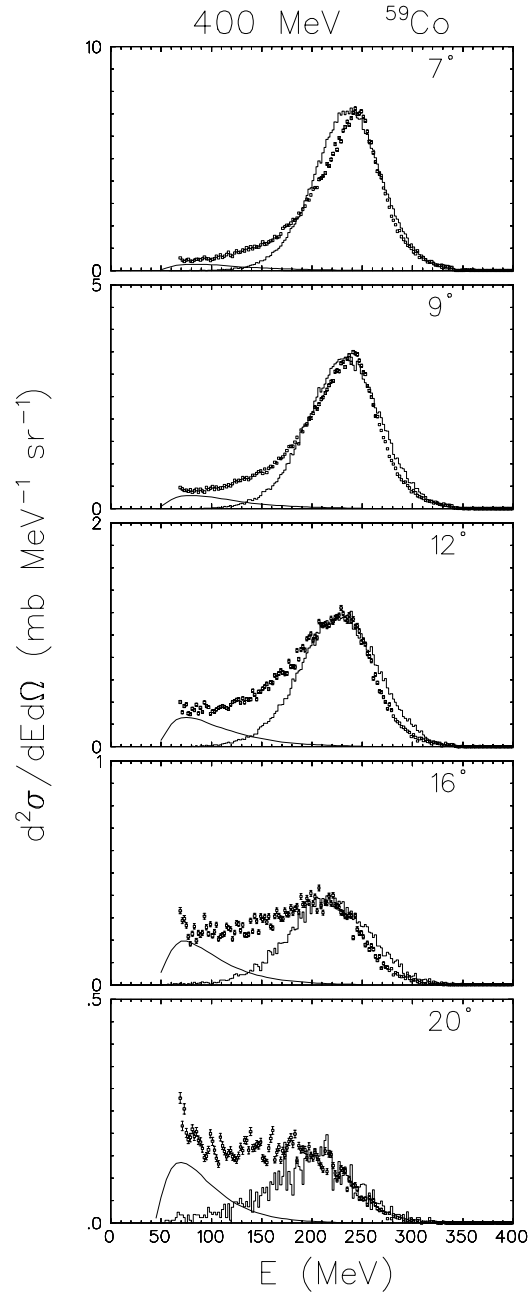

Fig. 5. Spectra of $^{8}Be_{gs}$ emitted between 7° and 20° in the interaction of 400 MeV ^{12}C with ^{59}Co. The experimental data are given by the open squares with error bars. The calculated break-up and coalescence spectra are given by, respectively, the histograms and the continuous lines.

squares and are compared to the theoretical predictions, given by the histograms and the full lines, which are evaluated as discussed below. However, the first calculations which we performed were based on the PWBA (discussed above and in refs. [3,9]) and satisfactorily reproduced the spectra of $^{8}Be_{gs}$ produced in the interaction of ^{12}C with ^{59}Co and ^{93}Nb at an incident energy of 100 MeV, using a local Coulomb correction to the ^{12}C and $^{8}Be_{gs}$ energy. The same was found to be nearly true for the Au target at incident energies of 200 MeV and higher, as shown in figs. 11 to 13 where the full line histograms give the predicted break-up spectra obtained with a local correction E_c to the ^{12}C energy of about 85 MeV, a value not much higher than the Coulomb barrier between the two ions at contact. At an incident energy of 100 MeV the required local correction to the ^{12}C energy was much smaller (about

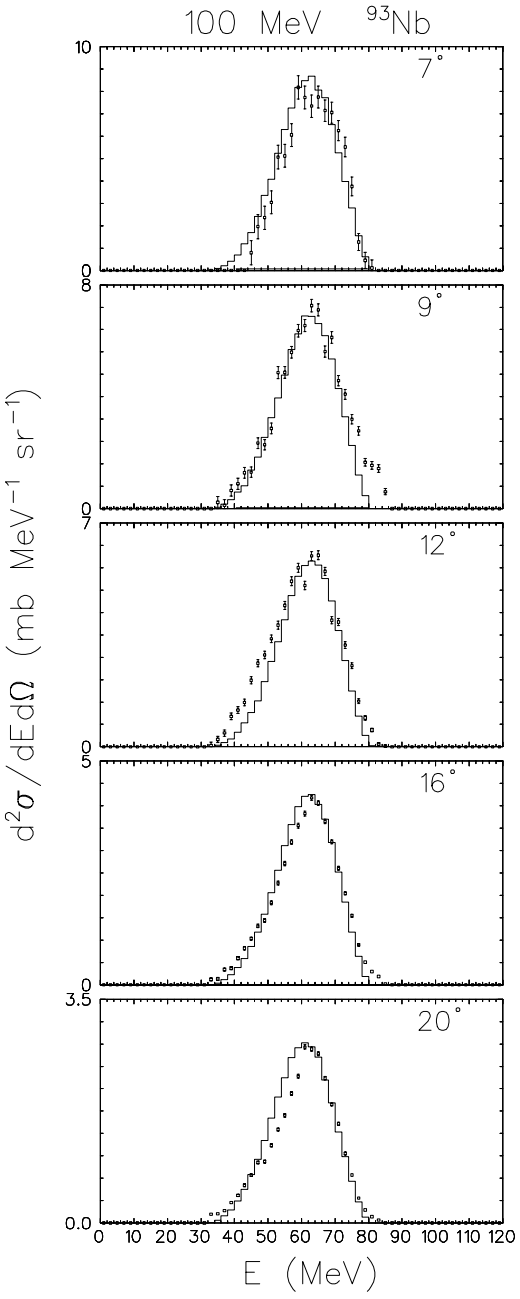

Fig. 6. Spectra of $^{8}Be_{gs}$ emitted between 7° and 20° in the interaction of 100 MeV ^{12}C with ^{93}Nb. The experimental data are given by the open squares with error bars. The calculated break-up spectra are given by the continuous line histograms.

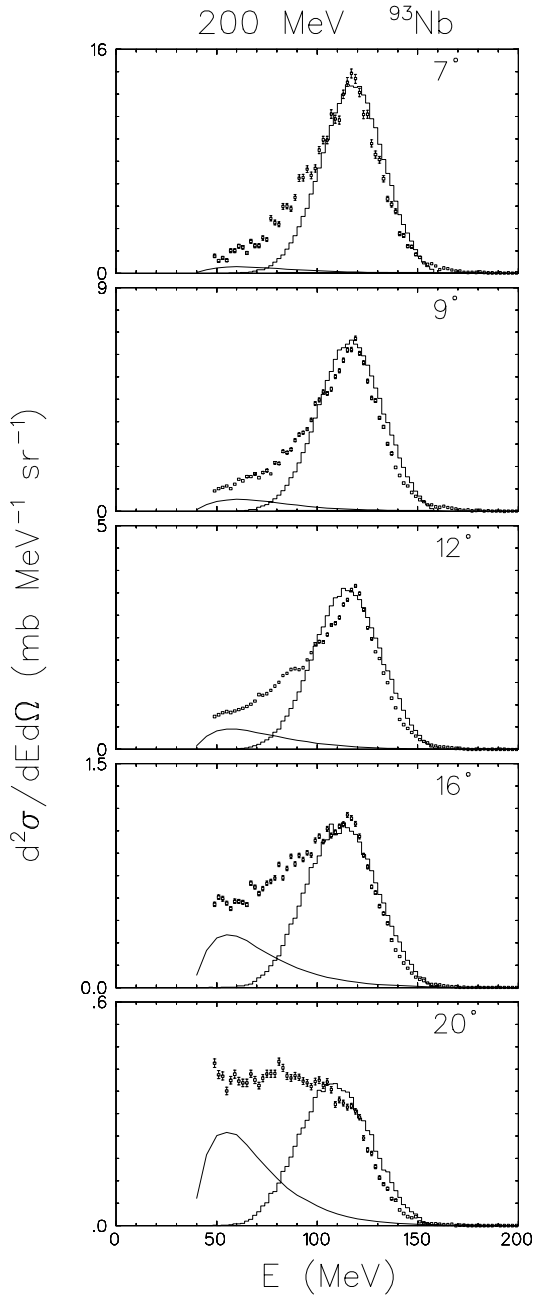

Fig. 7. Spectra of $^{8}Be_{gs}$ emitted between 7° and 20° in the interaction of 200 MeV ^{12}C with ^{93}Nb. The experimental data are given by the open squares with error bars. The calculated break-up and coalescence spectra are given by, respectively, the histograms and the continuous lines.

35 MeV) suggesting that presumably the break-up of ^{12}C occurs at larger distances where the Coulomb potential is correspondingly smaller.

However, when similar calculations were done at higher incident energies for ^{59}Co and ^{93}Nb, the projectile energy correction had to be increased with incident energy up to a value which at 400 MeV was larger by a factor of between 2 and 2.5 than the expected Coulomb correction. In order to illustrate this different behaviour, fig. 14 compares the experimental $^{8}Be_{gs}$ spectra (normalized to the same height) at 400 MeV and at an emission angle of 9°, for the ^{59}Co and ^{197}Au targets. In spite of the expected larger Coulomb correction to the ^{12}C energy, the average $^{8}Be_{gs}$ energy is larger in the case of ^{197}Au than in the case of ^{59}Co. The width of the spectrum for the interaction with ^{197}Au is also considerably smaller, as is expected in a pure break-up process.

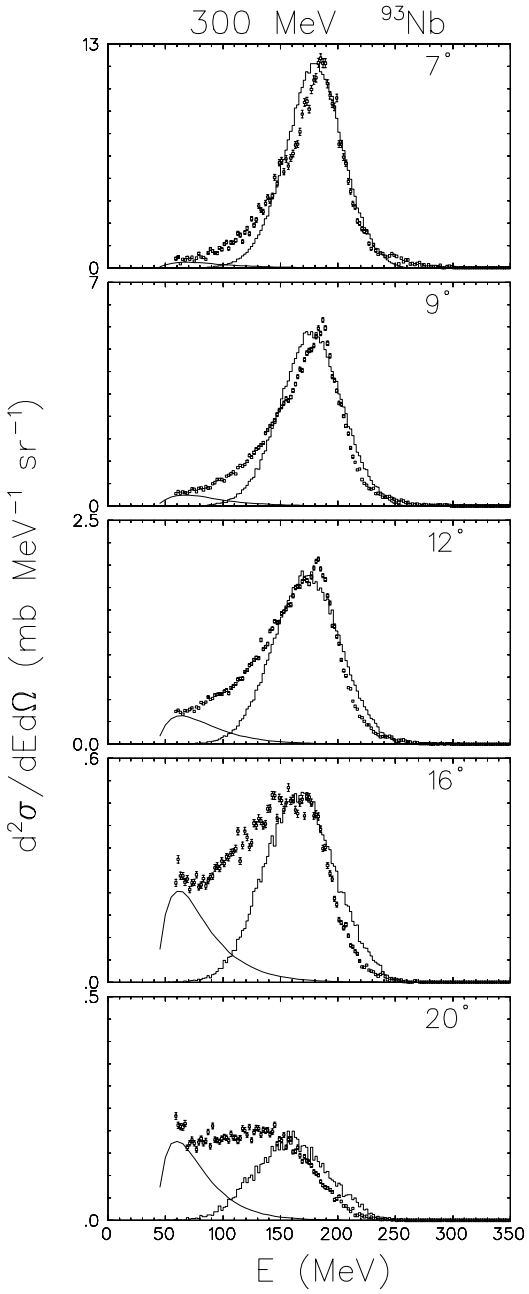

Fig. 8. Spectra of $^{8}Be_{gs}$ emitted between 7° and 20° in the interaction of 300 MeV ^{12}C with ^{93}Nb. The experimental data are given by the open squares with error bars. The calculated break-up and coalescence spectra are given by, respectively, the histograms and the continuous lines.

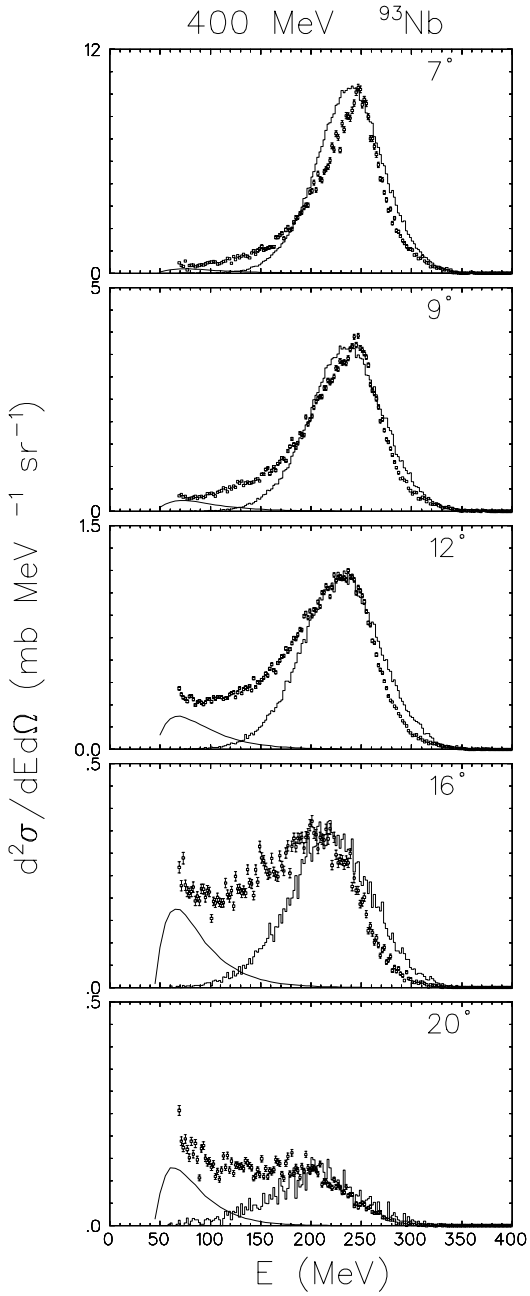

Fig. 9. Spectra of $^{8}Be_{gs}$ emitted between 7° and 20° in the interaction of 400 MeV ^{12}C with ^{93}Nb. The experimental data are given by the open squares with error bars. The calculated break-up and coalescence spectra are given by, respectively, the histograms and the continuous lines.

3.2 Theoretical analysis

In the Serber-McVoy-Hussein approximation [3,9,11,12] the spectrum of the observed fragment is given by

$$\frac{\mathrm{d}^2\sigma}{\mathrm{d}E\mathrm{d}\Omega} \propto P'P''|\psi(\mathbf{p})|^2, \qquad (1)$$

with

$$\mathbf{p} = \mathbf{P}' - (m_\mathrm{f}/m_\mathrm{P})\mathbf{P}. \qquad (2)$$

$\mathbf{P}$ and $\mathbf{P}'$ are, respectively, the momenta of the projectile and of the observed fragment, P'' the modulus of the momentum of the unobserved fragment and m_P and m_f are, respectively, the masses of the projectile and the observed fragment.

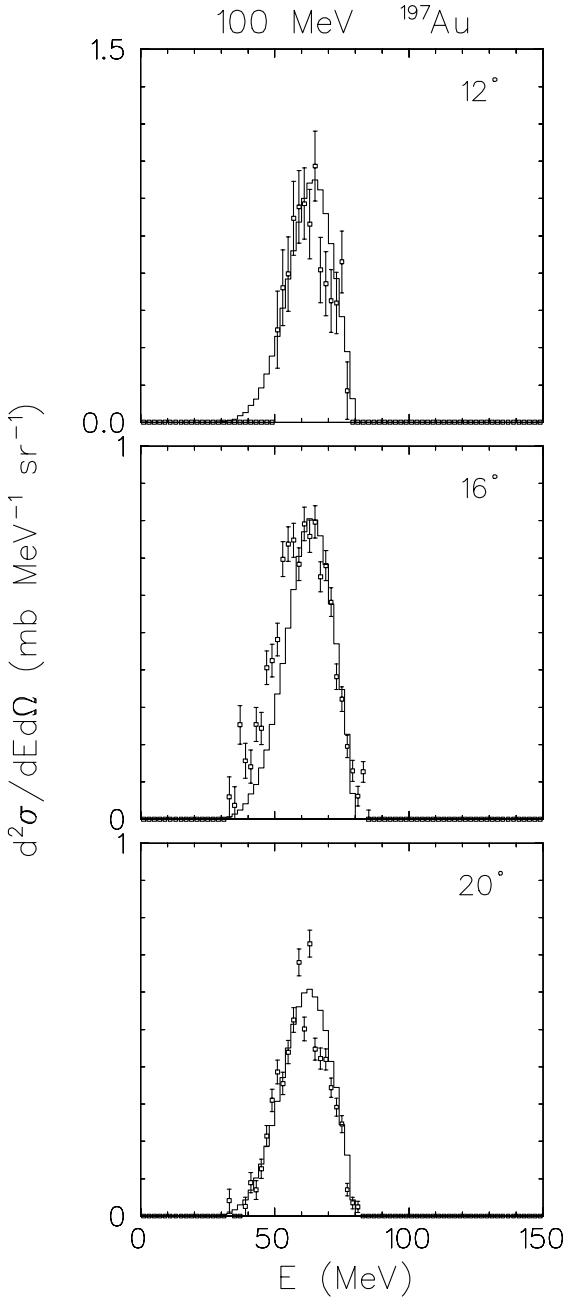

Fig. 10. Spectra of ^{8}Be$_{gs}$ emitted between 12° and 20° in the interaction of 100 MeV ^{12}C with ^{197}Au. The experimental data are given by the open squares with error bars. The calculated break-up spectra are given by the continuous line histograms.

The function $\psi(\mathbf{p})$ is the Fourier transform of the wave function describing the relative motion of the fragments within the projectile

$$\psi(\mathbf{p}) = \frac{1}{(2\pi\hbar)^{3/2}} \int \psi(r) \exp\left[-\frac{i}{\hbar}(\mathbf{p}\cdot\mathbf{r})\right] \mathrm{d}\mathbf{r}. \quad (3)$$

For $\psi(r) = R(r)/r$ we use a deuteron-like expression:

$$R(r) = A \sin Kr, \quad 0 < r \leq R\,,$$

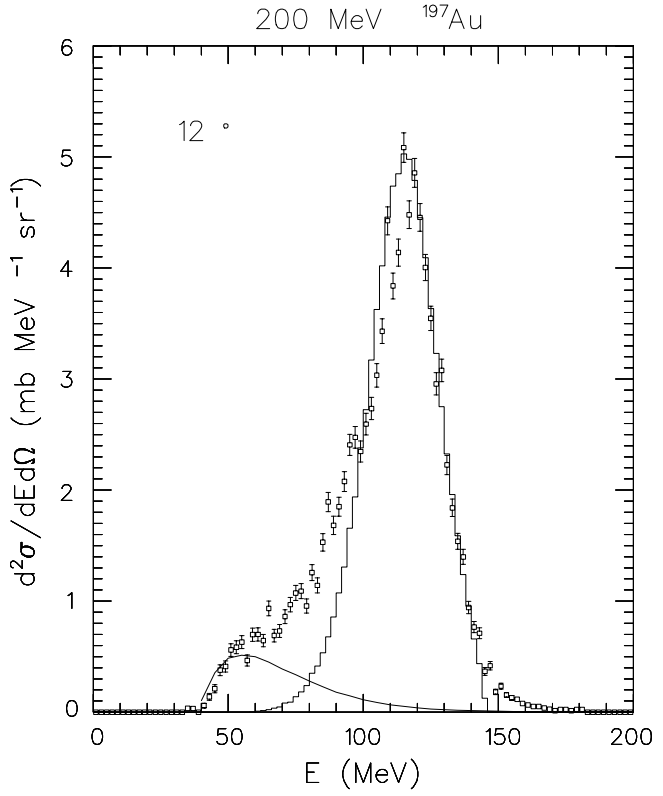

Fig. 11. Spectra of ^{8}Be$_{gs}$ emitted at 2° in the interaction of 200 MeV ^{12}C with ^{197}Au. The experimental data are given by the open squares with error bars. The calculated break-up and coalescence spectra are given by, respectively, the histogram and the continuous line.

$$R(r) = B\mathrm{e}^{-k_1 r}, \quad r > R. \quad (4)$$

If K and k_1 are known, the values of A, B and R are fixed by the matching and normalization conditions. At first we used $K = 1.32$ fm^{-1} and $k_1 = 0.97$ fm^{-1}, the values evaluated for a two cluster α-^{8}Be wave function assuming a square-well interaction potential 21 MeV deep and a separation energy of 7.367 MeV. The corresponding wave function is given by the dashed line in fig. 15. Subsequently, we decided to use a slightly different wave function with K and k_1 equal, respectively, to 1.64 and 0.84 fm^{-1} which is given by the full line in fig. 15. This wave function gave a slightly better reproduction of the angular dependence of the ^{8}Be break-up spectra, especially at the highest incident energy.

As discussed before, one should use Coulomb corrected values for $\mathbf{P}$, $\mathbf{P}'$ and P''. However, as noted before, especially in the case of the lighter target nuclei and the higher incident energies, the average energies of the ^{8}Be fragments, which presumably are produced in the ^{12}C break-up, are distinctly smaller and the widths of their energy distributions distinctly larger than those evaluated in this way. To account for this, it has been suggested [14] that, *before* breaking up, ^{12}C may suffer a nonnegligible energy loss. Following this suggestion, we assume that as it moves in the field of the target nucleus, ^{12}C loses energy by excit-

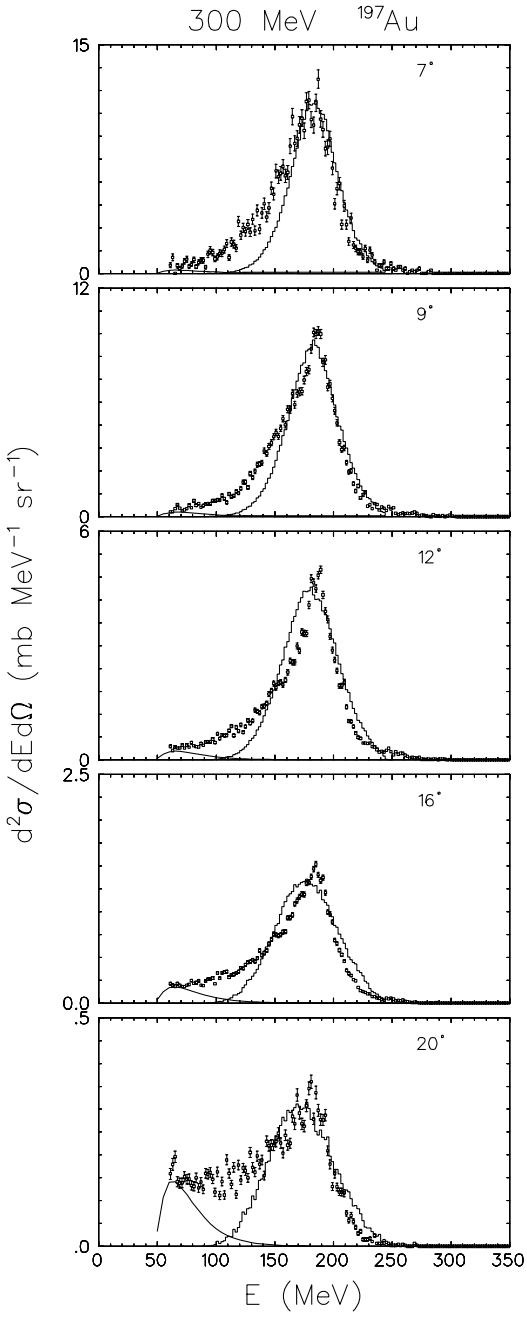

Fig. 12. Spectra of $^{8}Be_{gs}$ emitted between 7° and 20° in the interaction of 300 MeV ^{12}C with ^{197}Au. The experimental data are given by the open squares with error bars. The calculated break-up and coalescence spectra are given by, respectively, the histograms and the continuous lines.

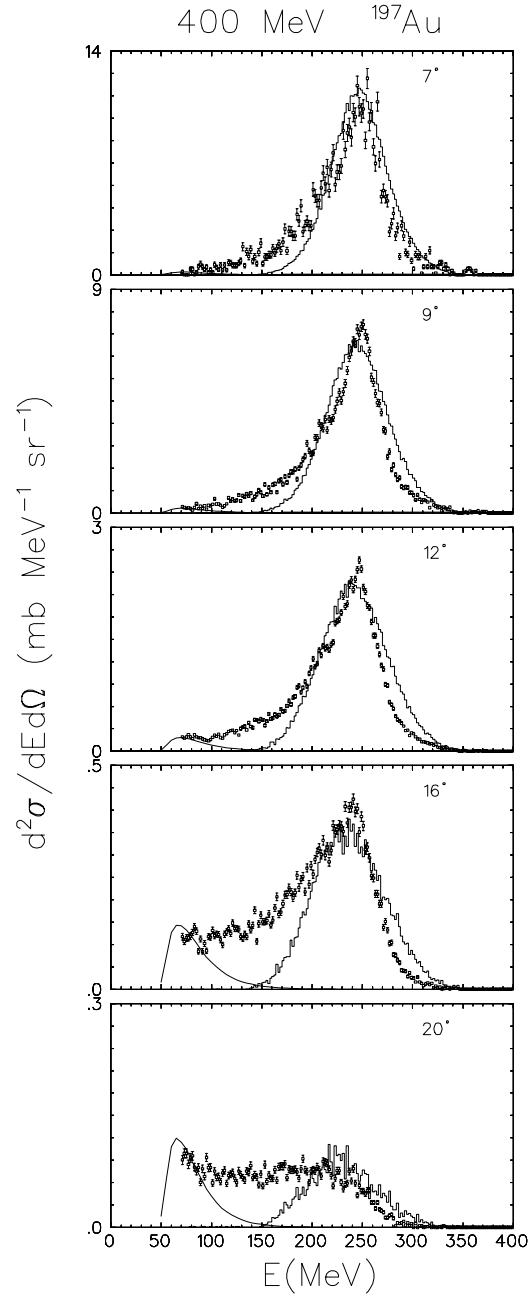

Fig. 13. Spectra of $^{8}Be_{gs}$ emitted between 7° and 20° in the interaction of 400 MeV ^{12}C with ^{197}Au. The experimental data are given by the open squares with error bars. The calculated break-up and coalescence spectra are given by, respectively, the histograms and the continuous lines.

ing the target, with the possibility of breaking up or transferring nucleons to the target nucleus in the course of this interaction. Friction dissipative interactions have been already considered in the literature (see for example [6–8, 10,21–25]) and it was shown that such interactions may lead to a considerable reduction of the kinetic energy of the projectile prior to other interactions in which it does not survive. Inelastic interactions, also leading to a considerable energy loss, have been also considered to account for the final-state interaction (or rescattering) of stable fragments produced in projectile break-up reactions [9].

In order to take into account this dissipative interaction between the ^{12}C and the target nucleus, we assumed, as a first approximation, that $P(E_{\rm l})$, the ^{12}C probability of surviving a break-up or a mass transfer, be equal to 1 for values, in the centre-of-mass system, of the projectile energy loss $E_{\rm l}$ smaller than a lower limit $E_{\rm l,min}$ (note that

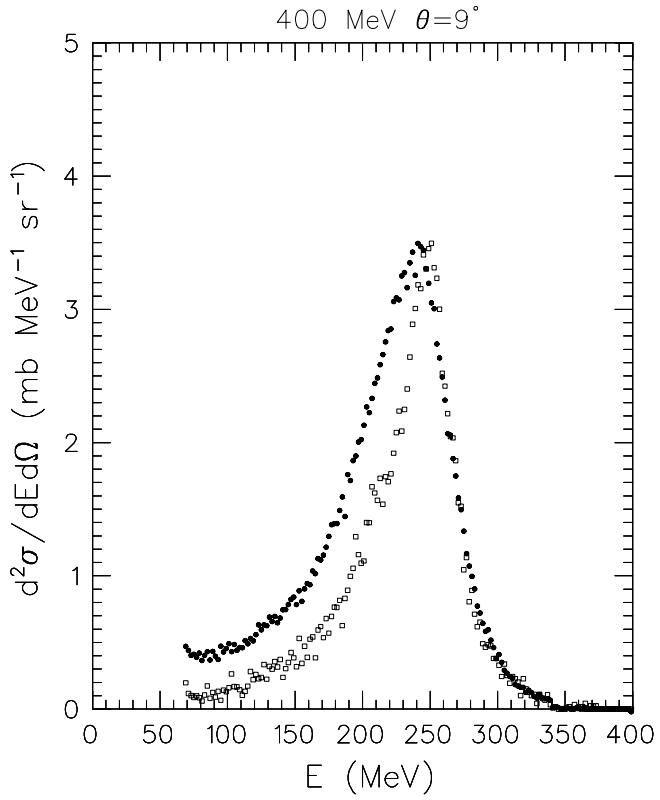

Fig. 14. Comparison of the spectra of $^{8}\mathrm{Be}_{\mathrm{gs}}$ emitted at 9° in the interaction of 400 MeV ^{12}C with, respectively, ^{59}Co (black circles) and ^{197}Au (open squares, normalized to the ^{59}Co spectrum for the sake of evidence).

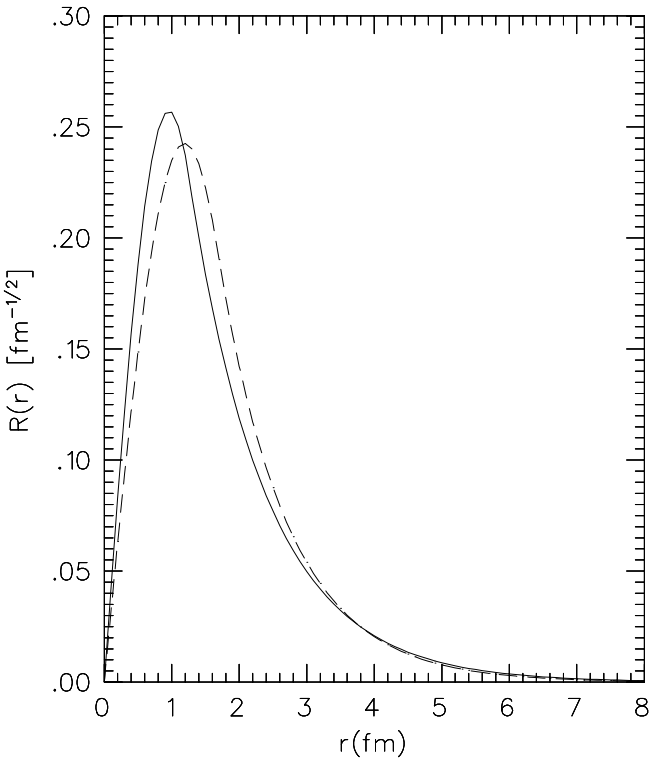

Fig. 15. Wave functions for the relative motion of one α and a $^{8}\mathrm{Be}_{\mathrm{gs}}$ within ^{12}C. For details, see the text.

E_{l} includes the energy lost by the Coulomb repulsion). If one assumes, for simplicity, a constant projectile energy loss per unit length $\mathrm{d}E/\mathrm{d}x = 1/k$ and a constant break-up and mass transfer probability k' per unit length when $E_{\mathrm{l}} > E_{\mathrm{l,min}}$, one immediately obtains for the ^{12}C survival probability $P(E_{\mathrm{l}})$ after a total energy loss E_{l}

$$P(E_{\mathrm{l}}) \propto \exp[-kk'(E_{\mathrm{l}} - E_{\mathrm{l,min}})]. \quad (5)$$

We further assumed that the spectrum $\mathrm{d}^2\sigma^S(E,E',\Theta)/\mathrm{d}E'\mathrm{d}\Omega$ (normalized to unity when integrated over the energy and solid angle) of the $^{8}\mathrm{Be}_{\mathrm{gs}}$ fragments of energy E' which are produced when the ^{12}C initial centre-of-mass kinetic energy E_0 is reduced to $E = E_0 - E_{\mathrm{l}}$, may still be evaluated in the Serber-McVoy-Hussein approximation correcting the observed fragment energy for the Coulomb repulsion at the moment of break-up. We then obtain for the break-up spectra of $^{8}\mathrm{Be}_{\mathrm{gs}}$,

$$\frac{\mathrm{d}^2\sigma}{\mathrm{d}E'\mathrm{d}\Omega}(E_0,E',\Theta) = \sigma_{\mathrm{bu}}\frac{\int_0^{E_0} P(E_{\mathrm{l}})S(E,E',\Theta)\mathrm{d}E_{\mathrm{l}}}{\int_0^{E_0} P(E_{\mathrm{l}})\mathrm{d}E_{\mathrm{l}}}, \quad (6)$$

where σ_{bu} is the angle and energy integrated cross-section for the production of $^{8}\mathrm{Be}_{\mathrm{gs}}$,

$$\begin{array}{ll} P(E_{\mathrm{l}}) = 1, & \text{for } E_{\mathrm{l}} < E_{\mathrm{l,min}}, \\ P(E_{\mathrm{l}}) = \exp[-kk'(E_{\mathrm{l}} - E_{\mathrm{l,min}})], & \text{for } E_{\mathrm{l,min}} \le E_{\mathrm{l}} \le E_0, \end{array}$$

and

$$\begin{array}{ll} S(E,E',\Theta) = 0, & \text{for } E_{\mathrm{l}} < E_{\mathrm{l,min}}, \\ S(E,E',\Theta) = \mathrm{d}^2\sigma^S(E,E',\Theta)/\mathrm{d}E'\mathrm{d}\Omega, & \text{for } E_{\mathrm{l}} \ge E_{\mathrm{l,min}}. \end{array}$$

This folding procedure is similar to that used by Hussein *et al.* [9] in order to account for a final-state inelastic interaction of the observed fragment. The energy dependence of the folding function (5) is not unrealistic, since the energy average of the inelastic scattering spectrum of light ions on nuclei and at energies like those we consider is rather accurately given by an expression of this type [9,26,27].

Table 1 gives the values of $E_{\mathrm{l,min}}$ and kk' which we used for reproducing the spectra (shown in figs. 2 to 9) of $^{8}\mathrm{Be}_{\mathrm{gs}}$ produced in break-up of ^{12}C interacting with ^{59}Co and ^{93}Nb. The table also gives the average energy loss of the projectile before break-up and the angle and energy integrated cross-sections for the production of $^{8}\mathrm{Be}_{\mathrm{gs}}$ in ^{12}C break-up. The local Coulomb correction to the $^{8}\mathrm{Be}_{\mathrm{gs}}$ kinetic energy was taken equal to 18.3 and 24.7 MeV in the case of the interaction of ^{12}C with, respectively, ^{59}Co and ^{93}Nb.

As mentioned before, in order to fit the $^{8}\mathrm{Be}_{\mathrm{gs}}$ spectra in the interaction of ^{12}C with ^{197}Au it was not necessary to use the previous folding procedure, but these spectra were rather satisfactorily reproduced using a single value for the local correction E_{c} to the projectile energy. These values are given in table 2 together with the angle and energy integrated break-up cross-sections. The

Table 1. Parameter values of $E_{l,min}$, kk', $\overline{\Delta E}$ (the calculated average energy loss of the projectile before break-up), the cross-sections for production of $^{8}Be_{gs}$ in ^{12}C break-up (σ_{bu}) and the complete fusion cross-section (σ_{cf}) for the interaction of ^{12}C with ^{59}Co and ^{93}Nb, as a function of the incident ^{12}C energy E_{inc}.

^{59}Co

E_{inc} (MeV)	$E_{l,min}$ (MeV)	kk' (MeV^{-1})	$\overline{\Delta E}$ (MeV)	σ_{bu} (mb)	σ_{cf} (mb)
100	23	0.115	32	56	1261
200	50	0.1	60	64	631
300	55	0.06	72	150	420
400	60	0.04	85	180	315

^{93}Nb

E_{inc} (MeV)	$E_{l,min}$ (MeV)	kk' (MeV^{-1})	$\overline{\Delta E}$ (MeV)	σ_{bu} (mb)	σ_{cf} (mb)
100	35	0.147	42	71	1533
200	55	0.128	63	67	766
300	55	0.058	72	151	511
400	60	0.038	86	182	383

Table 2. Parameter values of the local correction to the ^{12}C energy, E_c, the cross-section σ_{bu} for production of $^{8}Be_{gs}$ in ^{12}C break-up, and the complete fusion cross-section σ_{cf} for the interaction of ^{12}C with ^{197}Au, as a function of the incident energy E_{inc}.

E_{inc} (MeV)	E_c (MeV)	σ_{bu} (mb)	σ_{cf} (mb)
100	35	10	1364
200	85	67	1208
300	85	159	773
400	90	239	552

corresponding theoretical predictions are shown in figs. 10 to 13. The fact that E_c at the three highest incident energies is about 30% higher than the expected Coulomb corrections seems to suggest that also in this case, before breaking up, ^{12}C transfers a small amount of its energy to the target nucleus. In fact the use of a single value for E_c is equivalent to use in (6) $E_{l,min} \approx E_c$ and a value of $kk' \approx 0.3\,\text{MeV}^{-1}$. This value is considerably larger than the values used to reproduce the spectra of $^{8}Be_{gs}$ emitted in the interaction of ^{12}C with ^{59}Co and ^{93}Nb and with such a value the surviving probability $P(E_l)$ decreases so rapidly with increasing E_l that ^{12}C breaks up before losing an appreciable amount of energy. The local correction to the $^{8}Be_{gs}$ kinetic energies was taken equal to 39.1 MeV at incident ^{12}C energies exceeding 100 MeV. At 100 MeV, in agreement with the smaller value of E_c, the local correction to the $^{8}Be_{gs}$ kinetic energy was taken equal to 27.5 MeV. The reduced values for the projectile and observed fragment local corrections were interpreted as an indication that, at an incident energy of 100 MeV, the ^{12}C break-up on gold occurs at a larger distance from the target nucleus.

The present calculations can reproduce only the highest energy part of the $^{8}Be_{gs}$ spectra. In [9] it was suggested that in addition to break-up there may be a further contribution, at the lower emission energies, due to a process unrelated to break-up, which these authors attribute to a complex multistep pre-equilibrium process. In this work we assume that this contribution is due to the coalescence of nucleons during the thermalization of the composite nucleus created in the complete fusion of the projectile and the target. This is calculated [28] using the more recent version of the Boltzmann master equation theory which some of the present authors have developed [29]. The calculation is performed using the set of mass- and energy-dependent parameters which have been shown to reproduce a large set of experimental data [28–30] and the complete fusion cross-sections σ_{cf} given in tables 1 and 2. For the interaction of ^{12}C with ^{59}Co and ^{93}Nb, the values of σ_{cf} are those which we used in a previous study [31] and are very similar to those reported by ref. [32]. For the interaction of ^{12}C with ^{197}Au, the values of σ_{cf} are those given in [32]. The contribution to the measured spectra of $^{8}Be_{gs}$ produced by nucleon coalescence is given in figs. 2 to 13 by the full lines at the lower emission energies. It is noteworthy that the model does not predict any measurable yield of $^{8}Be_{gs}$ produced by nucleon coalescence at an incident energy of 100 MeV where contributions due to this mechanism have not been found experimentally. In these figures, the calculated break-up spectra are, at each angle, normalized to the data. The values of the normalizing factors are nearly the same at the lower incident energies (100 and 200 MeV) for all the three considered reactions. At the two higher incident energies the predicted break-up cross-sections decrease with increasing angle, more rapidly than the experimental ones. However, the discrepancy between the experimental and the calculated angular distributions, including the coalescence contribution, is not large even at these incident energies. This is shown in figs. 16 to 18 where the calculated angular distributions are compared to the experimental ones without any normalization. It is noteworthy that the theory predicts very similar angular

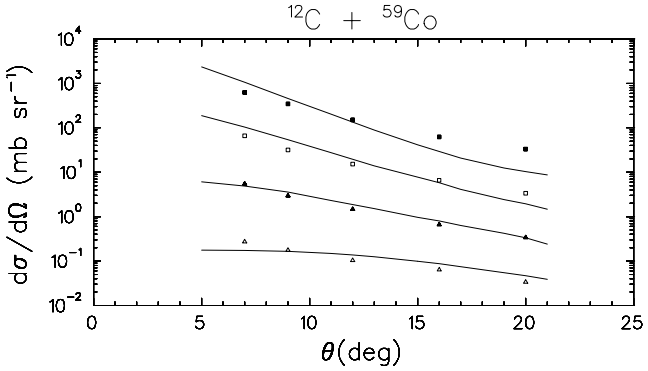

Fig. 16. Angular distributions of the energy integrated spectra of $^{8}Be_{gs}$ emitted in the interaction of 100, 200, 300 and 400 MeV ^{12}C with ^{59}Co. The upper angular distribution is that of $^{8}Be_{gs}$ emitted at the highest incident energy (400 MeV). Going from top to bottom the incident energy decreases progressively from 400 to 100 MeV and each angular distribution is scaled progressively by a factor of ten. The experimental angular distributions are given by the open and black symbols, the calculated ones (including both the break-up and the coalescence contributions) by the full lines.

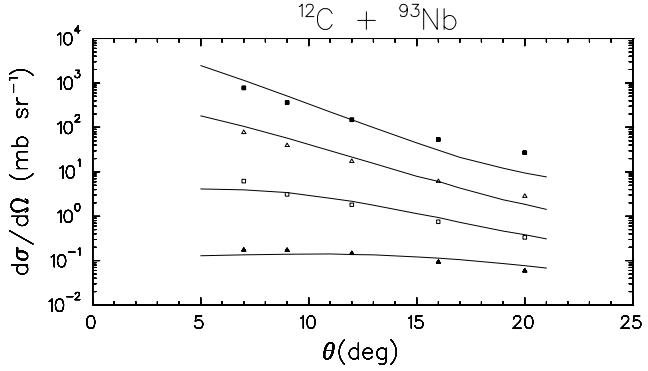

Fig. 17. Angular distributions of the energy integrated spectra of $^{8}Be_{gs}$ emitted in the interaction of 100, 200, 300 and 400 MeV ^{12}C with ^{93}Nb. The upper angular distribution is that of $^{8}Be_{gs}$ emitted at the highest incident energy (400 MeV). Going from top to bottom the incident energy decreases progressively from 400 to 100 MeV and each angular distribution is scaled progressively by a factor of ten. The experimental angular distributions are given by the open and black symbols, the calculated ones (including both the break-up and the coalescence contributions) by the full lines.

distributions for the three nuclei irrespective of their different mass and charge. This is in agreement with the experimental findings, as shown in fig. 19, where the theoretical and experimental angular distributions for the three nuclei are superimposed.

The decrease with incident energy of the values of kk', given in table 1 for the interaction of ^{12}C with both ^{59}Co and ^{93}Nb, seems to indicate that the probability of surviving break-up or mass transfer increases with increasing ^{12}C energy, so that it may lose a rather considerable amount of energy before breaking up. This does not seem to happen in the interaction of ^{12}C with ^{197}Au, suggesting

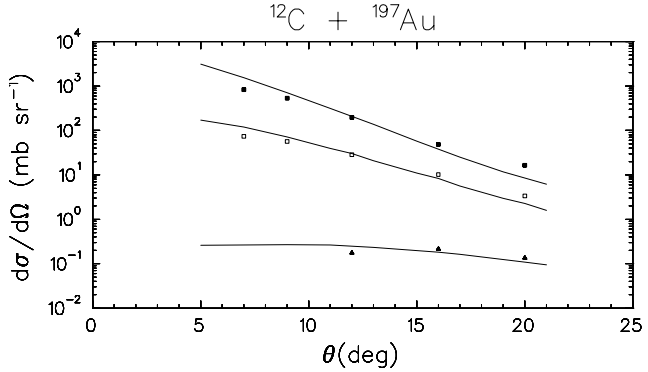

Fig. 18. Angular distributions of the energy integrated spectra of $^{8}Be_{gs}$ emitted in the interaction of ^{12}C with ^{197}Au. The upper, middle and lower angular distributions correspond to incident energies of, respectively, 400, 300 and 100 MeV. Going from top to bottom each angular distribution is scaled progressively by a factor of ten. The experimental angular distributions are given by the open and black symbols, the calculated ones (including both the break-up and the coalescence contributions) by the full lines.

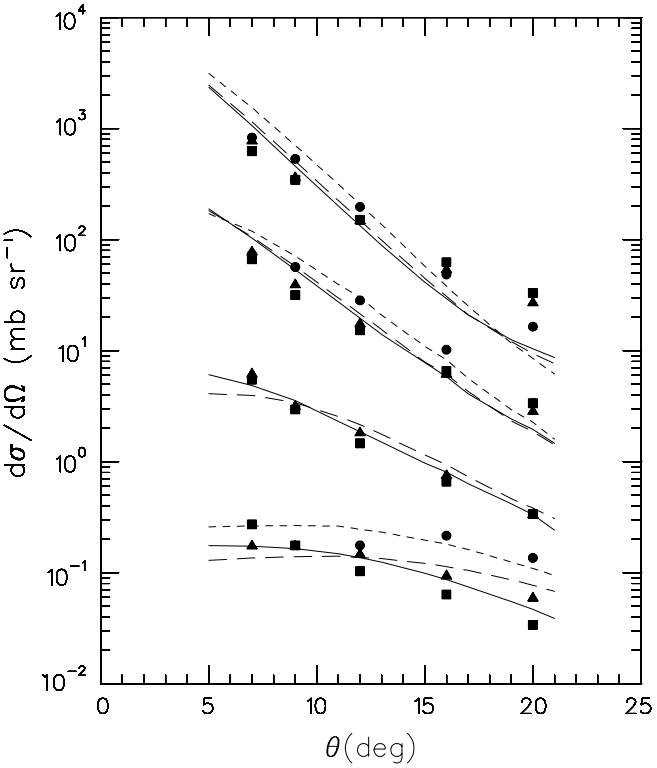

Fig. 19. Comparison of the angular distributions of the energy integrated spectra of $^{8}Be_{gs}$ for the three considered nuclei and the four considered incident energies. Going from top to bottom the incident energy decreases progressively from 400 to 100 MeV and each set of the angular distributions is scaled progressively by a factor of ten. The experimental angular distributions are given by the black symbols (squares: ^{59}Co; triangles: ^{93}Nb; circles: ^{197}Au). The theoretical distributions are given by the full (^{59}Co), long dash (^{93}Nb) and short dash (^{197}Au) lines.

that the survival probability of ^{12}C decreases with increasing Z.

4 Conclusions

The study of the production of $^{8}Be_{gs}$ in the interaction of ^{12}C with target nuclei of considerably different charge and also over quite a broad range of incident energies, provides a unique opportunity for investigating the mechanism of ^{12}C break-up. In fact, the experimental spectra of an unstable fragment such as $^{8}Be_{gs}$ are not contaminated by the contribution of other Be isotopes and the production of ^{8}Be in the first excited state can contribute only marginally to the measured spectra. In addition the $^{8}Be_{gs}$ instability makes it very improbable that it will survive a final-state interaction.

The experimental data suggest that, especially in the case of the lower mass nuclei and the highest incident energies which we have considered, when ^{12}C breaks up its energy may be significantly smaller than that expected considering only the Coulomb repulsion. This interpretation assumes that before breaking up, the ^{12}C projectile may lose energy by exciting the target nucleus. The amount of energy transferred in this way to the target nucleus seems to increase with increasing incident energy and decreasing target nucleus charge.

We wish to express our sincere gratitude to Dr. Tom Davinson of the University of Edinburgh for providing us with the Monte Carlo program UNIMONTE, various input and other relevant files, as well as useful communication to get the code operational. We thank also Simona Crippa for the help she gave in the analysis of the data and Roberto Bassini for technical support.

References

1. D.M. Brink, Phys. Lett. B **40**, 37 (1972).
2. T. Udagawa, T. Tamura, T. Shimoda, H. Frölich, M. Ishihara, K. Nagatani, Phys. Rev. C **20**, 1949 (1979).
3. K.W. McVoy, M. Carolina Nemes, Z. Phys. A **295**, 177 (1980).
4. H. Frölich, T. Shimoda, M. Ishihara, K. Nagatani, T. Udagawa and T. Tamura, Phys. Rev. Lett. **42**, 1518 (1979).
5. T. Udagawa, T. Tamura, B.T. Kim, Phys. Lett. B **82**, 349 (1979).
6. K. Möhring, T.Srokowski, D.H.E. Gross, H. Homeyer, Phys. Lett. B **203**, 210 (1988).
7. K. Möhring, T.Srokowski, D.H.E. Gross, Nucl. Phys. A **533**, 333 (1991).
8. H. Fuchs, K. Möhring, Rep. Progr. Phys. **57**, 231 (1994).
9. M.S. Hussein, K.W. McVoy, D. Saloner, Phys. Lett. B **98**, 162 (1981).
10. F. Guzman Martinez, R. Reif, Nucl. Phys. A **436**, 294 (1985).
11. R. Serber, Phys. Rev. **72**, 1008 (1947).
12. N. Matsuoka, A. Shimizu, K. Hosono, T. Saito, M. Kondo, H. Sakaguchi, Y. Toba, A. Goto, F. Ohtani, N. Nakanishi, Nucl. Phys. A **311**, 173 (1978).
13. C.K. Gelbke, C. Olmer, M. Buenerd, D.L. Hendrie, J. Mahoney, M.C. Mermaz, D.K. Scott, Phys. Rep. **42**, 311 (1978).
14. E.Gadioli, M.Cavinato, E.Fabrici, E.Gadioli Erba, R.Bassini, C.Birattari, S.Crippa, G.F.Steyn, S.V.Förtsch, J.J.Lawrie, F.M.Nortier, S.H.Connell, E.Sideras Haddad, J.P.F.Sellschop, A.A.Cowley, Eur. Phys. J. A **8**, 373 (2000).
15. S.L. Thomas, T. Davinson, A.C. Shotter, Nucl. Instrum. Methods A **288**, 212 (1990).
16. T. Davinson, A.C. Shotter, E.W. Macdonald, S.V. Springham, P. Jobanputra, A.J. Stephens, S.L. Thomas, Nucl. Instrum. Methods A **288**, 245 (1990).
17. E.W. Macdonald, A.C. Shotter, D. Branford, J. Rahighi, T. Davinson, N.J. Davis, Y. El Mohri, J. Yorkson, Nucl. Instrum. Methods A **317**, 498 (1992).
18. G.F. Steyn et al., in preparation.
19. E.W. Macdonald, *General Purpose Monte Carlo Simulation Code for Break-up Reactions*, UNIMONTE, University of Edinburgh (1988), unpublished.
20. F. Ajzenberg-Selove, Nucl. Phys. A **490**, 1 (1988).
21. W.U. Schröder, J.R. Huizenga, Ann. Rev. Nucl. Sci. **27**, 465 (1977).
22. M. Lefort, C. Ngo, Ann. Phys. (Paris) **3**, 5 (1978).
23. D.H.E. Gross, H. Kalinowski, Phys. Rep. **45**, 175 (1978).
24. G. Royer, Y. Raffray, A. Oubahadou, B. Remaud, Nucl. Phys. A **466**, 139 (1987).
25. A. Oubahadou, R. Dayras, G. Royer, J. Phys. G: Nucl. Phys. **17**, 1415 (1991).
26. R.R. Betts, S.B. DiCenzo, M.H. Mortensen, R.L. White, Phys. Rev. Lett. **39**, 1183 (1977).
27. M. Buenerd, D. Lebrun, J. Chauvin, Y. Gaillard, J.M. Loiseaux, P. Martin, G. Perrin, P. de Saintignon, Phys. Rev. Lett. **40**, 1482 (1978).
28. M. Cavinato, E. Fabrici, E. Gadioli, E. Gadioli Erba, A.M. Gritti, Z. Phys. A **347**, 237 (1994).
29. M. Cavinato, E. Fabrici, E. Gadioli, E. Gadioli Erba, G. Riva, Nucl. Phys. A **679**, 753 (2001).
30. C. Brusati, M. Cavinato, E. Fabrici, E. Gadioli, E. Gadioli Erba, Z. Phys. A **353**, 57 (1995).
31. E. Gadioli, M. Cavinato, E. Fabrici, E. Gadioli Erba, C. Birattari, I. Mica, S. Solia, G.F. Steyn, S.V. Förtsch, J.J. Lawrie, F.M. Nortier, T.G. Stevens, S.H. Connell, J.P.F. Sellschop, A.A. Cowley, Nucl. Phys. A **654**, 523 (1999).
32. W.W. Wilcke, J.R. Birkelund, H.J. Wollersheim, A.D. Hoover, J.R. Huizenga, W.U. Schröder, L.E. Tubbs, At. Data Nucl. Data Tables **25**, 389 (1980).